Chapter 6

Estimate of the thermal inertia of NEAs and assessment of the accuracy of thermal models

6.1 Foreword

To study the effects of surface roughness, thermal inertia and rotation rate on the thermal infrared emission of asteroids, a thermophysical model is developed throughout this chapter. We show that the thermal properties of the large majority of the NEAs in our database can be described by means of that model. Assuming that our objects have been observed with random orientation of their spin vectors with respect the illumination and the observing geometry, we derive a best-fit value of their thermal inertia of 550±100% J m^{-2} $s^{-0.5}$ K^{-1} or some 11 times that of the lunar soil. We show that this result has consequences of extreme importance on our understanding of the surface structures and the Yarkovsky effect on sub-kilometer -sized bodies.

6.2 Introduction

In Chapter 5 it has been shown that the value of the NEATM best-fit model parameter η is phase angle dependent and that there are marked differences between different NEAs in the value of η when observed at phase angle larger than 30-40 degrees. Beyond that phase angle, the distribution of the η-values appears to be bimodal with the large majority of objects showing η-values no larger than two and scattered around the straight line of equation $\eta=(0.011\pm0.002)\alpha+(0.92\pm0.07)$, where α is the phase angle. The NEATM η-value is inversely related to the observed color temperature, T_C, such that higher values of η imply lower values of T_C (see Eq. 5-1 and section 5.2).

In the NEATM, the beaming parameter η takes account of effects that alter the temperature distribution on the surface of the asteroid visible to the observer compared to that of a perfectly smooth non-rotating sphere. It has been assumed that this alteration is largely due to surface roughness and to the fact that all asteroids rotate and radiate part of the thermal infrared emission from the nigh-side. Surface roughness and rotation have competing effects on determining the final value of η. Macroscopic roughness tends to enhance the thermal infrared emission towards the Sun, causing the asteroid to appear with a color temperature hotter than that of a smooth sphere. The resulting η-value will thus be smaller than unity, when the object is observed at low phase angle. Rotation combines with the finite thermal inertia of the surface. Since asteroids spin, part of their thermal infrared radiation will be emitted from the night side. Conservation of energy implies that less radiation will be thus available for emission

on the sunward direction. The color temperature of the day-side hemisphere will appear consequently lower than the one of a non-rotating object and the η-value will be larger than unity. So, increasing roughness decrease η and increasing rotation or thermal inertia increase η.

It is clear that these considerations are valid when the asteroid is observed at low phase angles. Spencer et al. (1989) and Spencer (1990) have modeled the effects of thermal inertia, rotation rate and surface roughness on the thermal emission of main belt asteroids. They have derived η-values as a function of these parameters and of the sub-solar latitude. However, their studies were tailored to that class of asteroids and their calculation carried out at zero degree of phase angle only. The thermal effect of rotation depends not only on the object's thermal inertia, rotation rate and pole orientation, but also on its temperature. Since NEAs are closer to the Sun than what main belt asteroids are, their surfaces are hotter and differences are expected to show up in η-values derived for NEAs with respect to those obtained for MBAs for a given pole orientation, rotation rate and thermal inertia. Moreover, the possible effects on η of observing objects at large phase angle have to be studied. Results of observations discussed in this work, Chapter 5, indicate clearly that η varies with phase angle.

In Chapter 5 we have seen how the large majority of NEAs have η-values scattered around a straight line of equation $\eta=(0.011\pm0.002)\alpha+(0.92\pm0.07)$, where α is the solar phase angle. Delbo et al. (2003) noted that $\eta \approx 0.8$ appears to be valid at phase angles approaching zero, where the uncertainties associated with use of the STM, which assumes asteroids as non-rotating and a fixed η-.value of 0.756, are at a minimum. The fact that $\eta \rightarrow 0.756$ for $\alpha \rightarrow 0°$ suggests that the assumption of the STM of low thermal inertia (expected for an asteroid covered in dusty collisional debris) may be valid for "common" NEAs. Furthermore, the fact that no object was observed at a low phase angle for which η is large (> 1.2) suggests that NEAs with high thermal inertia (indicative of a rocky surface or course regolith) are relatively uncommon[20].

However, the present work revises up the η_0 value, namely the value of η at $\alpha=0°$, to about 0.9 by including further observations to the linear fit of Fig. 5.3. Moreover, new IRTF observations obtained for the NEA 5381 Sekmeth have revealed η-values that appear to fill the gap between the color temperatures shown by NEAs with common thermal properties and the "anomalous" low color temperature displayed by 2100 Ra-Shalom. Is the conclusion that the large majority of NEAs have low thermal inertia still valid in the light of these new results?

[20] A low value of thermal inertia is compatible with a surface covered with an insulating layer of regolith as in the case of the Moon. The lunar soil has a thermal inertia between 40 and 50 J m^{-2} $s^{-0.5}$ K^{-1}. Large main belt asteroids have thermal inertia even lower: about 30% that of the moon.

The fact that NEAs appear not to have high thermal inertia is, actually, quite contrary to expectations and it is remarkable that this seems to apply even for relatively small objects in the few-100-m size range: how can such small objects retain with their low gravities insulating regoliths of collisional debris? Furthermore, the presence of three "anomalous" asteroids, including the only two binary asteroids in the Keck data set, displaying color temperatures apparently exceptionally low ($\eta \approx 3$) when observed at large phase angles (>50°) shows the large diversity of surface structure present in the NEA population. An explanation of this behavior in terms of high thermal inertia requires values exceeding that of bare rock, which is clearly unrealistic. Alternatively, the surfaces in these cases may be unusually rough and irregular leading to enhanced thermal emission in the sunward direction ("beaming") and consequently less (and cooler) emission observed at high phase angles.

Information on the thermal inertia and surface structure of NEAs may be obtained from the variation in effective color temperature, with solar phase angle. However, a clear picture of this dependence is at present not available. More complex thermophysical modeling is in the need for describing the variation the color temperature as a function of the illumination and viewing geometry in terms of physical quantities such as thermal inertia and macroscopic surface roughness. Unfortunately, effects of thermal inertia combine with those of rotation rate, of spin vector orientation and of macroscopic surface roughness to yield the final observed color temperature and is not clear if separating out the contribution of each component is possible on the basis of the observations we have gathered so far. However, results that may come up from applying thermophysical models to observations of NEAs have several important consequences to gain insight into the surface properties of this population of minor bodies.

An estimation of the thermal inertia of NEAs allows to quantifying systematic errors in diameters and albedos inherent in the use of simple thermal models which make assumptions about the surface temperature distributions and/or neglect the thermal infrared flux arising from the non-illuminated fraction of the body. Moreover, knowing asteroids thermal properties is directly relevant to studies of the Yarkovsky effect, namely the drift in the orbital motion of small asteroids due to the reactive force of emitted thermal radiation. Dynamicists invoke this effect to explain the delivery of km-sized asteroids from the main belt into near-Earth orbits. It is also crucial for the assessment of the impact risk from potentially hazardous NEAs, such as 1950 DA. However, the magnitude of the effect depends critically on assumed thermal properties of asteroid surfaces, and is significantly reduced in the case of bodies having low thermal inertia (Bottke et al., 2002).

In this chapter a thermophysical model, which includes the effects of thermal inertia, rotation and surface roughness, is developed and used to study the dependence of the η-value with the solar phase angle, α. Furthermore, this model will allow us to produce thermal infrared emission spectra of synthetic asteroids with different surface properties and under different illumination and observing geometries. By fitting thermal models to these spectra we will study the reliability of the derived radiometric diameters and albedos and the likely presence of systematic errors.

6.3 Thermophysical model components

The thermophysical model implemented in this study is a variant of that developed by Spencer et al. (1989) and Spencer (1990). In our thermophysical model the synthetic asteroid is made of a mesh of triangular facets[21]. Several shapes of different complexity can be handled as shown in Fig. 6.1. For each facet the one-dimensional heat diffusion differential equation is solved numerically. This differential equation depends on the so-called thermal parameter Θ which is a product of the surface thermal inertia and the asteroid rotation rate (see Spencer et al., 1989).

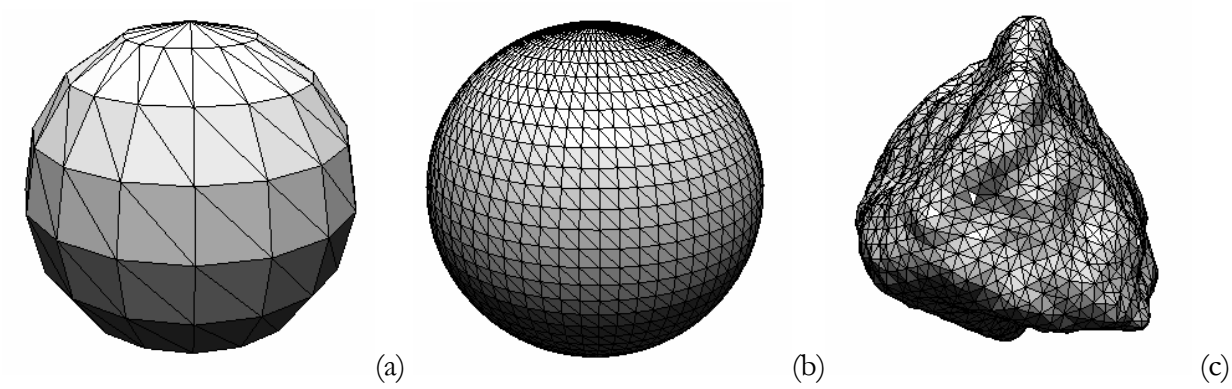

Fig. 6.1 The model herewith implemented can handle spheres of with a small (a) or a large number of elementary triangular facets (b). General shapes can also be modeled as in the case of the radar model of the NEA 6489 Golevka (c).

To simulate surface roughness, an energy balance equation is solved for temperature within spherical section craters. One crater is generated for each tile of the mesh. Surface roughness can be adjusted by changing the opening angle of the craters, the density of the crater distribution, or a combination of the two. However, Emery et al. (1998) has shown that if surface roughness is measured in terms of the mean surface slope, $\overline{\theta}$, according to the parameterization introduced by Hapke (1984), emission spectra

[21] Part of the code that implements the thermophysical model has been developed in collaboration with Stefano Mottola.

are function of the $\bar{\theta}$ parameter only and not of the crater opening angle and crater surface density. We recall here that

$$\tan\bar{\theta} = \frac{2}{\pi}\int_0^{\pi/2} a(\theta)\tan\theta d\theta \qquad (6\text{-}1)$$

where θ is the angle of a given facet from horizontal, and a(θ) is the distribution of surface slopes.

The thermophysical model includes

1. heating by direct sunlight, including the effect of shadowing;
2. subsurface diurnal heat flow normal to the local surface;
3. heating by sunlight multiply scattered within the crater;
4. self-heating by reabsorption of thermal radiation from other parts of the crater;

The model calculates disk-integrated thermal infrared flux summing up the flux from the crater of each tile of the mesh, f_i^{crat}, weighted with the crater density ϱ_{crat} and the thermal flux arising from the flat part of the tile f_i^{tile} multiplied by $(1-\varrho_{crat})$:

$$F(\lambda) = \sum_{i=1}^{N_t} \rho_{crat} f_i^{crat}(\lambda, \mu_i, \mu_i', \alpha) + (1-\rho_{crat}) f_i^{tile}(\lambda, \mu_i, \mu_i') \qquad (6\text{-}2)$$

where μ_i is the cosine of the direction to the observer and μ'_i is the cosine of the direction to the Sun with respect to the normal of the i-th tile of the mesh and α is the solar phase angle. Not all elements in all craters will be illuminated by direct sunlight, nor will they all be visible from the observer. The flux originating from each carter is calculated taking into account the visibility of crater elements. The procedure we have used to test if a crater element is in shadow, which is exactly analogous to the procedure to test for visibility, is similar to that developed by Emery et al. (1998).

6.4 Thermal Inertia and the heat diffusion within spherical craters

The assumption of instantaneous thermal equilibrium with sunlight at all points on the surface of an asteroid (Equilibrium Model, hereafter EM) result in a temperature distribution which depends on the solar incident angle only μ_s and fall to zero beyond the terminator (see Eqs (2-8) and (2-12)).

However, if heat conduction is important the surface can respond not instantaneously to variation of the insolation energy. The temperature is not only a function of the albedo and the heliocentric distance but depends also on the previous thermal history of the surface and part of the energy is radiated from

the dark side of the body. Solutions of the one-dimensional heat flow equation depend on the thermal inertia parameter,

$$\Gamma = \sqrt{\rho \kappa c}\,, \tag{6-3}$$

which combines the material surface density ϱ, the material conductivity ϰ and the specific heat capacity c.

However, the effect of thermal inertia is coupled to rotation rate. An asteroid rotating slowly with high thermal inertia displays a similar temperature distribution of one rotating very rapidly but with a lower thermal inertia. The degree to which the surface of an asteroid can respond to changes in insolation can be characterized by a single parameter. This is the so-called thermal parameter Θ, which combines rotation rate, thermal inertia and surface temperature and consequently depends on the heliocentric distance of the body. The thermal parameter is given by Eq. (6-4).

$$\Theta = \frac{\Gamma \sqrt{\omega}}{\varepsilon \sigma T^3}\,, \tag{6-4}$$

where ε is the emissivity, ω is equal to 2π divided by sidereal rotational period of the asteroid T_{SID}, and σ is the Stefan-Boltzman constant. T is the temperature of the asteroid surface.

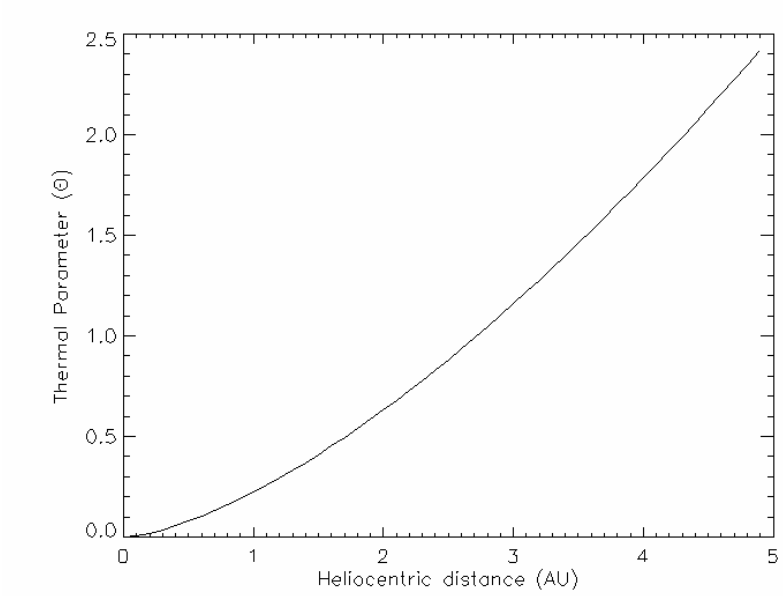

Fig. 6.2 Plot of the thermal parameter Θ as a function of the heliocentric distance. The thermal inertia has a quasi-lunar like value (Γ = 40 J m^{-2} s^{-1} K^{-1}). The bolometric bond albedo A is equal to 0.05; emissivity ε equal to 1 and asteroid sidereal rotation period T_{SID} equal to 5 hours. Note that for a given value of Γ and T_{SID}, objects in near-Earth space (r~1AU) have smaller Θ-values than objects more distant from the Sun.

In the literature, it is often said that an asteroid is a "slow-" or "fast-rotator" if $\Theta=0$ or $\Theta\rightarrow\infty$ respectively. For a lunar-like thermal inertia, the typical value of Θ for a main-belt asteroid falls in the range 0.1, 2.0. The temperature of the object plays a strong role: cooler objects with constant rotation rate and thermal inertia radiate less of their heat on the day hemisphere and more on the night hemisphere. Fig. 6.2 shows the dependence of the thermal parameter, Θ, as a function of the heliocentric distance. It is interesting to note that for a given value of Γ and T_{SID}, the thermal parameter Θ assumes smaller values the closer an object is to the Sun: the temperature distribution of a NEA is more similar to the EM temperature distribution than the temperature distribution of an object further away from the Sun, in the main belt or in the Jupiter-Trojan region.

The thermophysical model solves the one-dimensional heat diffusion differential equation for each tile of the mesh:

$$\frac{\partial T(X,t)}{\partial t} = \omega \frac{\partial^2 T(X,t)}{\partial X^2} \tag{6-5}$$

with the following boundary condition at the surface:

$$\sqrt{\omega}\Gamma\left(\frac{\partial T(X,t)}{\partial X}\right)_{X=0} = \omega\sigma T^4(0,t) - (1-A)\frac{S_0}{r^2}\mu_i'(t) \tag{6-6}$$

where $S_0 = 1374$ J m^{-2} s^{-1} is the solar energy flux at 1 AU from the sun, r is the solar distance in AU, μ'_i is the cosine of the solar zenith angle of the i-th tile of the mesh, A is the bolometric Bond albedo, σ is the Stefan–Boltzmann constant, ε is the emissivity. See Spencer el al. (1989) for further details.

Within craters, for each crater element Eq. (6-5) holds true and describes correctly the vertical heat flow. However, the boundary condition equation has to include heating by sunlight multiply scattered within the crater and self-heating by reabsorption of thermal radiation from other parts of the crater. In symbols:

$$\begin{aligned}\sqrt{\omega}\Gamma\left(\frac{\partial T_i(X_i,t)}{\partial X_i}\right)_{X_i=0} &= \omega\sigma T_i^4(0,t) - (1-A)(1-S_i)\frac{S_0}{r^2}\mu_i'(t) + \\ &- \varepsilon\sigma\sum_{j\neq i} f_{ij}T_j^4(0,t)\cos(\beta_{ij}) - E_{ref}(0,t)\end{aligned} \tag{6-7}$$

where μ'_i is the cosine of the solar zenith angle of crater element i and E_{ref} is the energy contributed from reflected solar radiation. Further, f_{ij} is the fraction of element j's sky subtended by element i, and β_{ij} is the angle between element i's normal and the line connecting elements i and j. S is a shadowing term

which is equal to 1 if the element is in shadow and equal to zero if the element is illuminated by direct sunlight. The second term on the right hand side of Eq. (6-7) represents heating by direct sunlight, the third term represents heating by thermal radiation emitted by other sections of the crater wall, and the first term represents thermal radiation emitted by element i. This equation is iteratively solved for each crater element to find the equilibrium temperature of each of the elements within the crater (see Emery et al., 1998).

Because heat conduction parallel to the surface is ignored, our thermophysical model results are independent of the scale of the craters, provided they are larger than the diurnal skin depth l_S which is given by:

$$l_S = \sqrt{\frac{k}{\rho c \omega}} \tag{6-8}$$

Spencer (1990) noted that in the case of main belt asteroids the value of l_S is of the order of some centimeters-millimeters assuming reasonable values for the density, heat capacity and heat conduction of the asteroid surface material. The heat diffusion process is highly localized on a diurnal timescale, implying that the application of simple one-dimensional vertical heat conduction models should be valid.

6.5 Numerical simulations

The purpose of this study is to model the effect of macroscopic surface roughness, thermal inertia and rotation rate on the thermal infrared emission and on the surface color temperature, for an object in near-Earth space as a function of the illumination and observing geometry. In particular we will do that by studying the dependence of the η-value derived by the NEATM (i.e. the color temperature) as a function of the phase angle. The reliability of the NEATM derived radiometric albedos and diameter as a function of the thermal parameter Θ and the macroscopic roughness $\bar{\theta}$ will be also derived.

To this end, synthetic thermal infrared spectra have been generated at different solar phase angles using a spherical shape mesh made of 184 elementary triangular facets. Each spectrum, which depends on Θ, $\bar{\theta}$ and the phase angle, α, has been treated a single observation and the NEATM has been used to fit the flux data and derive the diameter, the albedo and the η-value of the synthetic asteroid.

In this simulation, the Sun and the observer are in the equatorial plane of the asteroid which is placed at 1.0 AU of distance from both the observer and the Sun. Physical parameters of the synthetic asteroid are: Sidereal rotational period T_{SID}=6 hours; diameter D=2km; bolometric Bond albedo A=0.05;

geometric visible albedo, p_V=0.128; resulting absolute magnitude H=16.334. The model does not include the effects of scattered thermal radiation and therefore assumes the emissivity equals to 1.

Each simulation starts with all the tiles of the mesh and all craters elements at a constant temperature. The solution to the heat diffusion problem is found numerically. The subsurface is divided into 32 slabs of thickness 0.25 × l_s. The deepest subsurface element is therefore 8 times beneath the skin depth (see Eq. (6-9)). The model calculates the heat flow from each slab to the next in successive increment of time δt using the discrete equivalent of Eq. (6-5):

$$T(X,t+\delta t) = T(X,t) + \left(\frac{2\pi\delta t}{(\delta X)^2 T_{SID}} \right) \left(T(X+\delta X,t) - 2T(X,t) + T(X-\delta X,t) \right) \qquad (6\text{-}10)$$

We choose the fewest number of time steps that gave a stable numerical solution. This value is of the order of 300 time steps per rotation for value of Θ>1, but it can become as large as 1500 for Θ<0.1. The asteroid is then let to spin for a number of rotations until the diurnal temperature stabilizes and has forgotten the initial conditions.

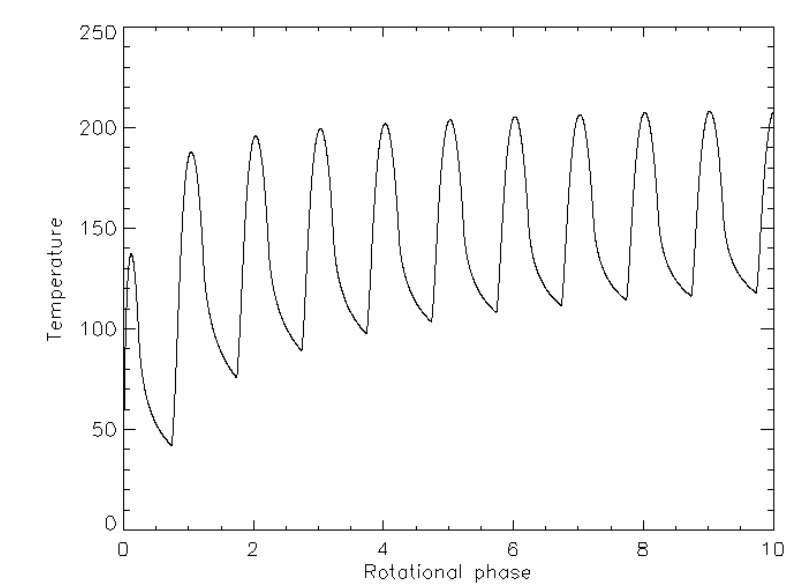

Fig. 6.3 The temperature of an equatorial tile of the spherical mesh monitored during the "warming up" phase. In this case the temperature of all the tiles of the mesh has been set equal to 0 K as starting conditions. After a few rotations the temperature stabilizes to within 0.5-1.0 K.

The temperature profile as a function of time, i.e. the asteroid rotational phase, has been monitored on an equatorial facet and on one of the four element on the floor of an equatorial crater during the warm

up phase, which can take up to 10-50 full rotations (depending on the value of Θ) until the temperature profile stabilizes (see Fig. 6.3).

Once the warming up process has been completed, a final rotation of the object allows the final solution to the surface temperature distribution to be derived. Fig. 6.4 shows the diurnal temperature profiles for an object with sub-solar latitude equal to zero as a function of the thermal parameter Θ.

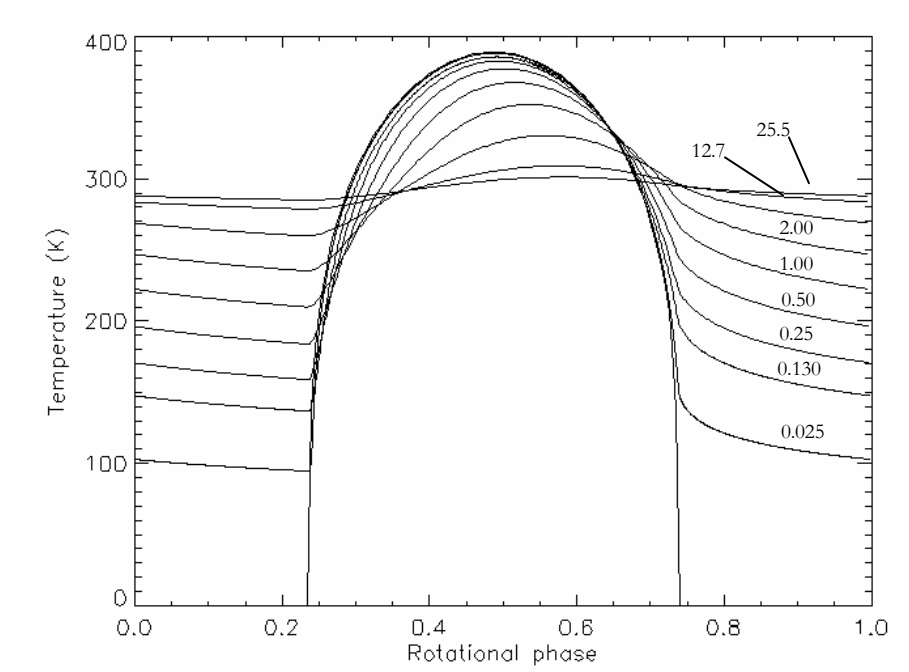

Fig. 6.4 Diurnal temperature profiles for an object with sub-solar latitude equal to zero as a function of the thermal parameter Θ.

Although these simulation have been carried out for a given rotational period of 6 hours by changing the thermal inertia, the results of the experiment depends actually on the thermal parameter Θ. Fig. 6.5 allows the thermal parameter Θ to be estimated for different rotational periods and different thermal inertias for an asteroid in near earth space.

A discrete set of wavelengths at 5.0, 8.0, 10.3, 12.5 and 20 μm has been adopted to sample the infrared spectra in the range 5 – 20 μm. Those wavelengths roughly correspond to the central wavelengths of narrow band filters used to carry out the ground-based observations discussed in the Chapter 3 of this study. A spectrum has been generated every ten degrees of phase angle from -90° (morning side) to 90° (afternoon side) for a set of values of the thermal inertia Γ = [5, 25, 50, 100, 200, 400, 900, 2500, 5000] J m^{-2} $s^{-0.5}$ K^{-1}. Those values of thermal inertia corresponds to Θ = [0.025, 0.13, 0.25, 0.50, 1.00, 2.00, 4.60, 12.70, 25.5] for the rotational period of 6 hours assumed for the synthetic

asteroid. The model has been run for several degree of macroscopic roughness: $\bar{\theta}$ =[0, 5, 10, 20, 58] degrees.

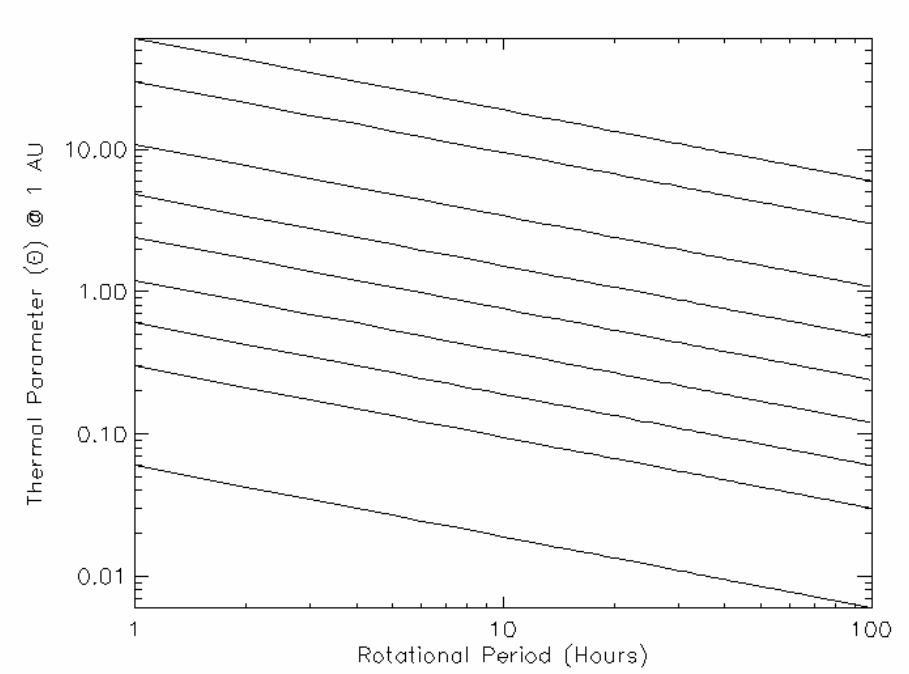

Fig. 6.5 This plot allows the thermal parameter Θ to be estimated given the thermal inertia Γ and the asteroid rotational period in hours. From the bottom of the figure to the top, the lines refers to the following values of Γ = [5, 25, 50, 100, 200, 400, 900, 2500, 5000] J m^{-2} $s^{-1/2}$ K^{-1}. The typical lunar-like value for Γ is about 40-50 m^{-2} $s^{-1/2}$ K^{-1}.

For each observation of the synthetic asteroid the NEATM has been used to fit the synthetic spectrum and in the next section, results of the simulations are presented.

6.6 Results of the simulations

6.6.1 Effects of thermal inertia and rotation rate on the theoretical dependence of the NEATM η-value as a function of the phase angle

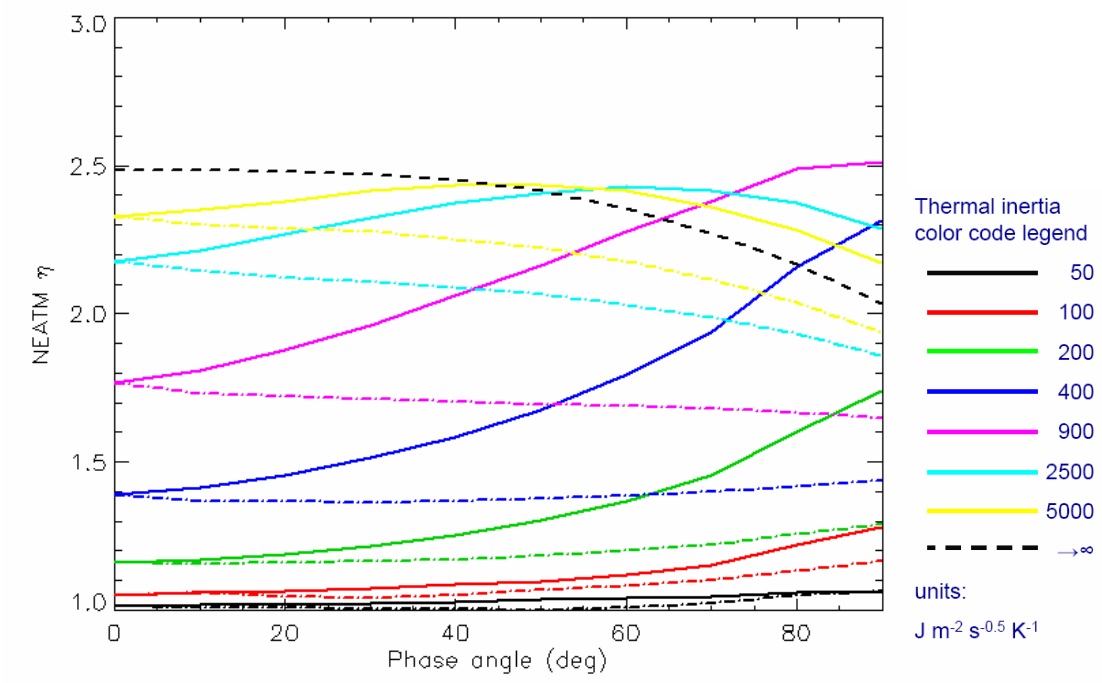

Fig. 6.6 NEATM derived beaming parameter η as a function of the phase angle and thermal parameter Θ. The sun and the observer are in the equatorial plane of the synthetic asteroid. Different colors are used for different values of Θ: η-values derived for Θ=0.25 are coded with black color; those obtained for Θ=0.50 are coded with red; green is used for Θ=1.00 with; blue for Θ=2.00; pink for Θ=4.60; light-blue for Θ=12.70 and yellow for Θ=25.5. Note that there are two curves for each value of the thermal parameter Θ: continuous curves refer to those η-values derived by observing the morning side of the asteroid, whereas dashed-dotted curves indicate those η-values obtained observing the afternoon side. Curves obtained for Θ=0.025 and 0.13 are not plotted since the derived η-values are constant with phase angle and their values between 1 and 1.05. The dotted black curve represents the expected η values for an FRM-like (Θ→∞) asteroid.

Fig. 6.6 shows the theoretical dependence of the NEATM best-fit η parameter for a smooth asteroid as a function of the phase angle for different values of the thermal parameter Θ. For each value of Θ, two curves are plotted. Continuous curves refer to those η derived by observing the cooler morning side of the asteroid, whereas dashed-dotted curves indicate those η-values obtained observing the warmer afternoon side.

We note that for values of Θ smaller than 0.5 (red curves), the value of η is small (<1.3) and rather constant up to phase angles as large as 90°. We remind here that the black colored curves correspond to

a lunar-like thermal inertia for a rotational period of six hours. No large variations of the η-value are visible for $\Theta$when the morning rather than the afternoon hemisphere of the asteroid is observed. Such variations are usually within the typical error bars of the NEATM derived η-values (see Chapter 5 and in particular Fig. 5.3). However, for larger Θ values, (i.e. Θ>1.0 – the green curves) such variation of the color temperature with the observing and illumination geometry appear. Moreover, large values of the thermal parameter correspond to η-values as large as 1.5 at phase angles approaching zero indicating a surface temperature distribution much cooler than the one expected by the EM. As Θ increases, the η-value at α=0° increases up to a maximum value of about 2.5 for $\Theta\rightarrow\infty$ which correspond to a FRM-like surface temperature distribution. It is worth to point out, how for very large values of the thermal parameter, the temperature of a surface element is constant through day and night and the "morning" η curve collapses on top of the "afternoon" one.

Note that beyond 50°-60° of phase angle, asteroids with Θ roughly larger than four can have η-values higher than an object with an FRM-like temperature distribution.

Fig. 6.6 indicates that thermal inertia and direction of rotation of NEAs can be estimated on the basis of the dependence of η with the phase angle if observations at large phase angle before and after oppositions are carried out. Since we expect to be able to derive η-values with an accuracy of about 30% (this is the mean relative error affecting the determination of η in the database of our observations), the thermal inertia of a NEA might be derived if its Θ-value is larger than one.

In this simulation the asteroid sub-solar latitude was always zero. If this is not the case, the surface temperature distribution deviates less from the EM one, as the sub-solar latitude approaches 90°. Our thermophysical model allows the surface temperature distribution to be calculated for whatever observing and illumination geometry. We have thus simulated the case of an asteroid which sub-solar latitude was varied from zero to ninety degrees, with an obliquity of 0° and observed at phase angles between -90° and 90°. Our simulations indicate that the larger the sub-solar latitude is, the smaller is the amplitude of the difference between the "afternoon" and the "morning" curves and the smaller is the η-value derived by NEATM. Finally, if the Sun shines above one of the asteroid poles, the temperature distribution is analogue to the EM one for whatever value of the thermal parameter Θ. Resulting η-values will be equal to 1 for every observing direction. So, given the value of Θ, for arbitrary illumination and observing geometries, expected η-values will range between 1 and the corresponding "morning" curve of Fig. 6.6.

6.6.2 Effects of surface roughness on the theoretical dependence of the NEATM η-value as a function of the phase angle

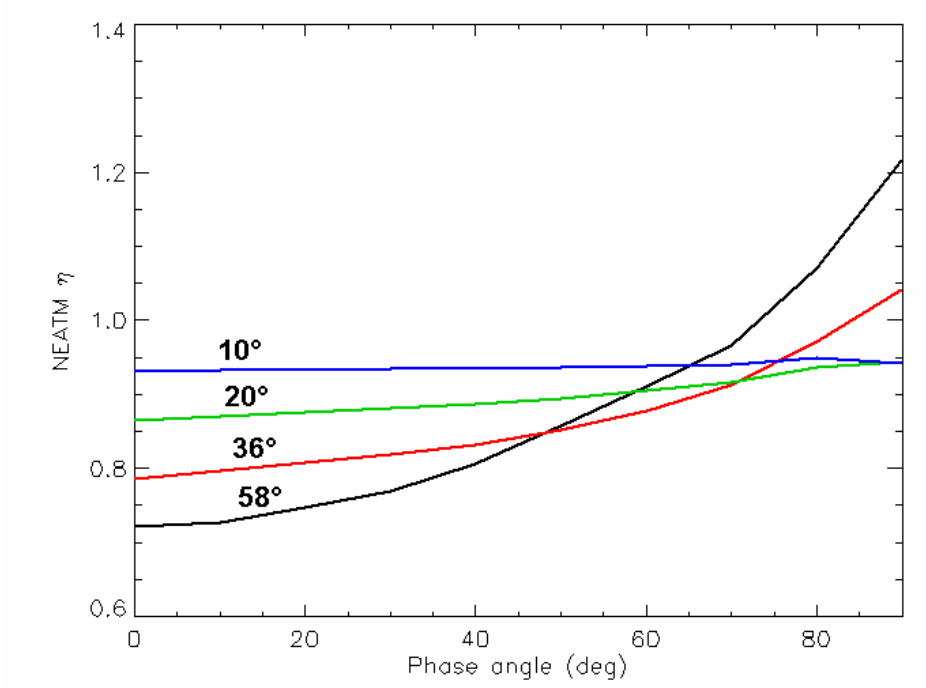

Fig. 6.7 NEATM derived η parameter as a function of the phase angle and macroscopic surface roughness $\bar{\theta}$. The sun and the observer are in the equatorial plane of the synthetic asteroid. The thermal parameter Θ is equal to 0. Different colors are used for different values of $\bar{\theta}$: η-values derived for $\bar{\theta}$=58° are coded with black color; those obtained for $\bar{\theta}$=36° are coded with red; for $\bar{\theta}$=20° with green and for $\bar{\theta}$=10° with blue.

Fig. 6.7 shows the theoretical dependence of the NEATM best fit η parameter as a function of the phase angle for different values of the macroscopic surface roughness $\bar{\theta}$. As it was expected, roughness increases the color temperature, T_C, of the surface when the asteroid is observed at small phase angles: i.e. $\eta < 1$. However, while for small values of $\bar{\theta}$, T_C is constant with the phase angle, for very rough surfaces the color temperature decreases as the phase angle increases. Since the thermal parameter Θ for this asteroid is equal to zero, no variation of the Fig. 6.7 curves are expected with sub-solar latitude. The temperature distribution is symmetrical with respect to the sub-solar point.

6.6.3 Combined effects of thermal inertia, rotation rate and surface roughness on the theoretical dependence of the NEATM η-value as a function of the phase angle

In this section we study the combined effects of thermal inertia, rotation rate and surface roughness of the thermal emission of NEAs and we derive the dependence of the NEATM best-fit parameter η on these physical parameters.

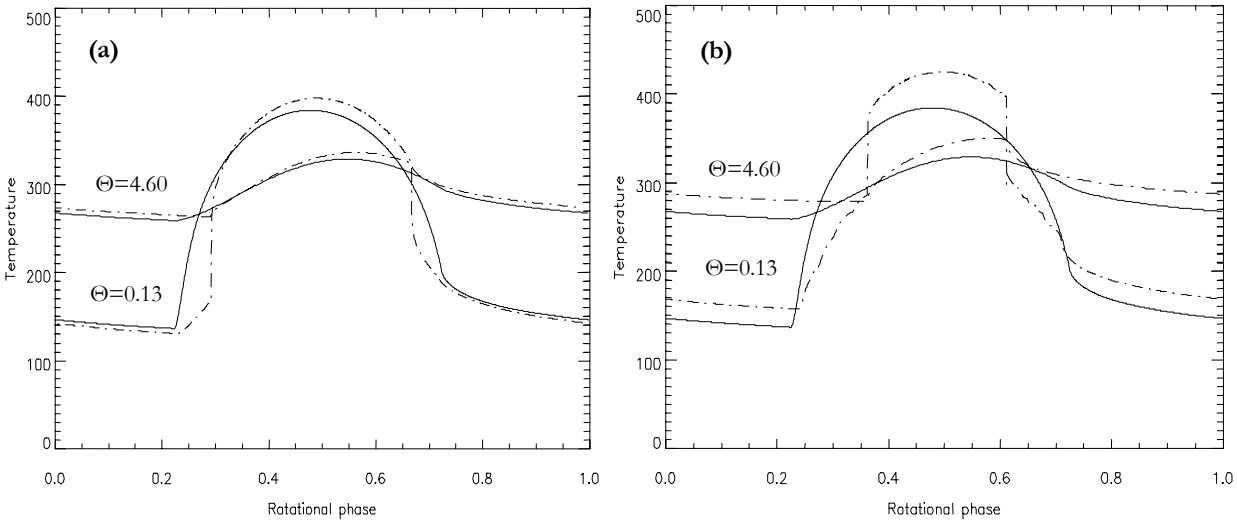

Fig. 6.8 Continuous line: diurnal temperature profiles for an equatorial tile of an object with sub-solar latitude equal to zero. Dashed-dotted line: diurnal temperature profiles for one of the four tiles on the floor of an equatorial crater with opening angle equals to 45° (a) and with opening angle equals to 90° (hemispherical crater).

Spencer (1990) has shown how the midday temperature across an equatorial crater varies with Θ. He has highlighted that for Θ=0 there is a large temperature enhancement on the floor of the crater compared to the nearby horizontal surface. Fig. 6.8 shows the diurnal temperature profile of one of the four tiles on the floor of an equatorial crater with respect to the temperature of the surrounding smooth surface for two different values of the thermal parameter Θ i.e. Θ=4.60 and Θ=0.13, as shown by the labels of Fig. 6.8. It is interesting to note that for large values of Θ, the temperature of the bottom of the crater is almost always higher than the temperature of the surrounding surface (i.e. the dashed-dotted is always above the continuous line). This effect, already visible in the case of a 45° crater, becomes significantly stronger for a 90° (hemispherical) crater. In this latter case our thermophysical model calculates a difference of more than 20° compared to the surrounding horizontal surface. This effect is due to the strong self-heating by reabsorption of thermal radiation from other parts of the crater. Furthermore, for large thermal inertias and or rotation rate, our thermophysical model indicates that a

surface heavily cratered by deep depressions appears hotter than a smooth one even if observed from the night side.

The observed color temperature, derived by fitting the NEATM on disk the integrated thermal infrared synthetic spectra generated by means of our thermophysical model, is a function of the thermal parameter Θ, the macroscopic surface roughness $\bar{\theta}$, the illumination and the observing geometry. So, in general we can write that

$$\eta \equiv \eta\left(B_{SS}, r, B_{SE}, \Delta, \alpha, \Theta, \bar{\theta}\right), \tag{6-11}$$

where B_{SS} is the latitude of the sub-solar point and B_{SE} the latitude of the sub-Earth point on the asteroid reference frame. r is the heliocentric distance, Δ the geocentric distance and α the phase angle. However, if the asteroid has sub-solar latitude equal to zero and viewed equator-on, at 1 AU from the Sun and the Earth, the dependence of the η-value on the illumination and the observing geometry is a function of the phase angle α only i.e.

$$\eta \equiv \eta(\alpha, \Theta, \bar{\theta}). \tag{6-12}$$

To study the function of Eq 6-10, we have run our thermophysical model for the set of values of Θ and $\bar{\theta}$ as described in section 6.5 and derived the η-value by fitting the NEATM on thermal infrared spectra generated at phase angles between -90 (morning side) and 90 (afternoon side) degrees of phase angle every 10°. Fig. 6.9 shows the functional dependence of η with α for different values of Θ and $\bar{\theta}$. The numerical values of η, calculated on a fixed grid of points in the α-Θ-$\bar{\theta}$ space, have been stored in a three-dimensional array. Fig. 6.10 shows η-values on sections of this three-dimensional data volume at constant values of the macroscopic surface roughness parameter $\bar{\theta}$.

At small phase angle (α<20°), for a given degree of roughness, η is determined by the magnitude of the thermal parameter Θ: the higher Θ is, the larger the η value, until the limiting value of 2.5 for Θ→∞ is reached. Moreover, it appears that the values of the NETAM best fit parameter η are not very sensitive to variation of the surface macroscopic roughness. According to Spencer (1990), our model calculations show that the small values of η seen in the case of the Moon and most large main belt asteroids (η~0.7-0.8) can be matched only by very rough surface models.

For α>20° and Θ>2.0 the morning η curves separate out from the afternoon ones and very different color temperature are observed by looking at the two opposite hemisphere of the object. The morning-afternoon effect has a maximum for Θ roughly equals to 5. For smaller values of the thermal parameter, the surface temperature distribution resembles that of the EM, whereas for large values of Θ (i.e. Θ>10)

the temperature distribution becomes smoothed out in longitude and constant throughout day and night.

At intermediate phase angles, i.e. $30°<\alpha<60°$, the morning curves, calculated for a given value of the thermal parameter, can cross the afternoon curves calculated for a different Θ value. This fact does not allow the Θ parameter to be estimated when the color temperature is derived at a certain phase angle, if the direction of rotation is not known.

At large phase angle (e.g. $\alpha>70°$) surface roughness contributes to a large extent to the final observed color temperature of the asteroid: note that large η-values (~3) at large phase angles ($\alpha\sim80°$) are compatible with a highly cratered surface ($\overline{\theta}=58°$) and moderate Θ parameter ($\Theta \sim 1 – 2$). Very rough and irregular surfaces lead to a high degree of "beaming" of thermal radiation in the sunward direction and correspondingly less and cooler radiation is emitted at high phase angles. However, for large thermal inertia and/or rotation rates, deep crates behave like a trap for the thermal energy and consequently the contribution of the roughness in decreasing the observed color temperature of the surface at large phase angles become less significant. Under such observing conditions, i.e. for $\alpha>70°$, the η-values cannot be used to determine unambiguously the values of the thermal and roughness parameters, even if the direction of rotation of the asteroid is known.

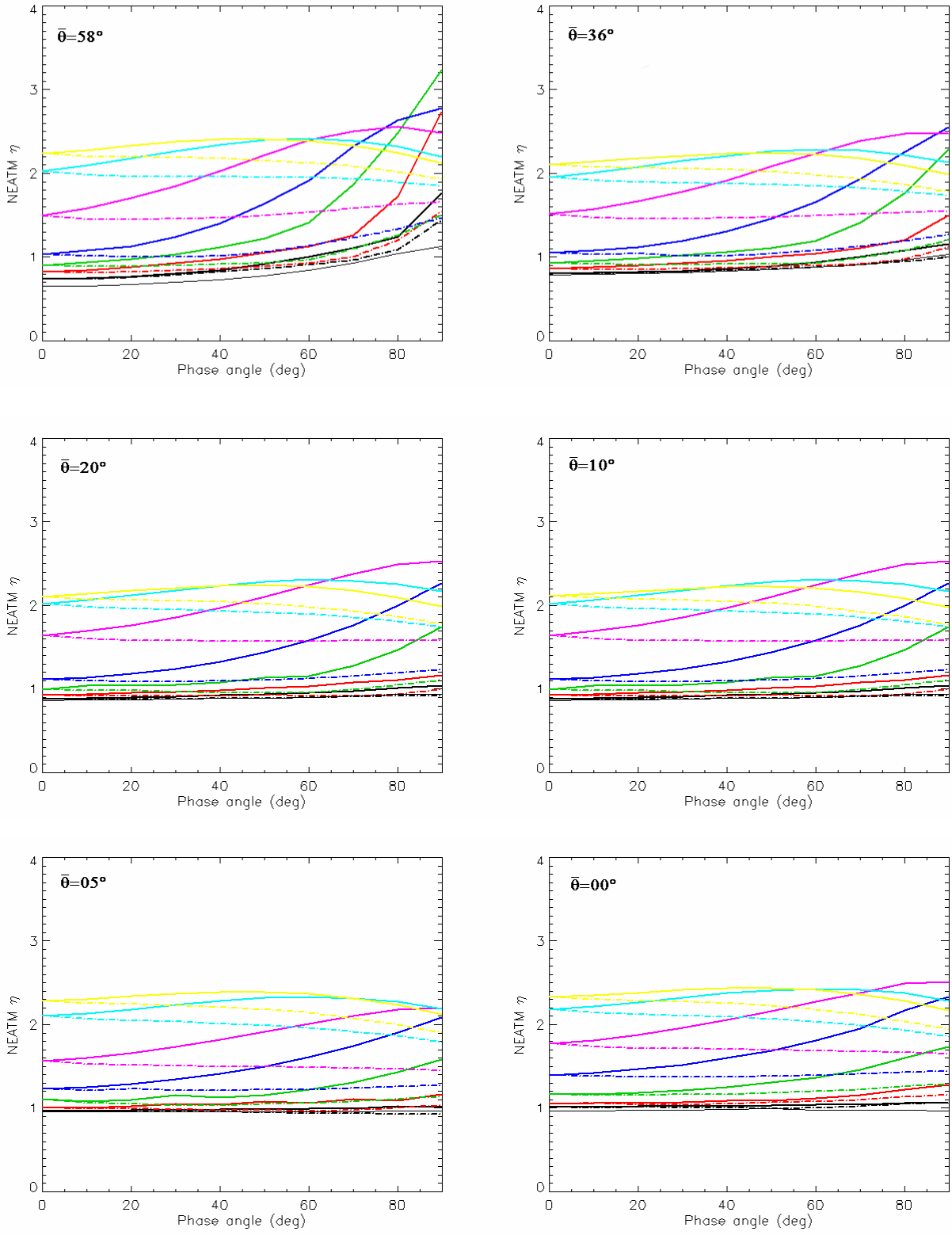

Fig. 6.9 Combined effects of thermal inertia, rotation rate and surface roughness on the theoretical dependence of the NEATM η-value with the phase angle. See Fig. 6.6 for the color codes.

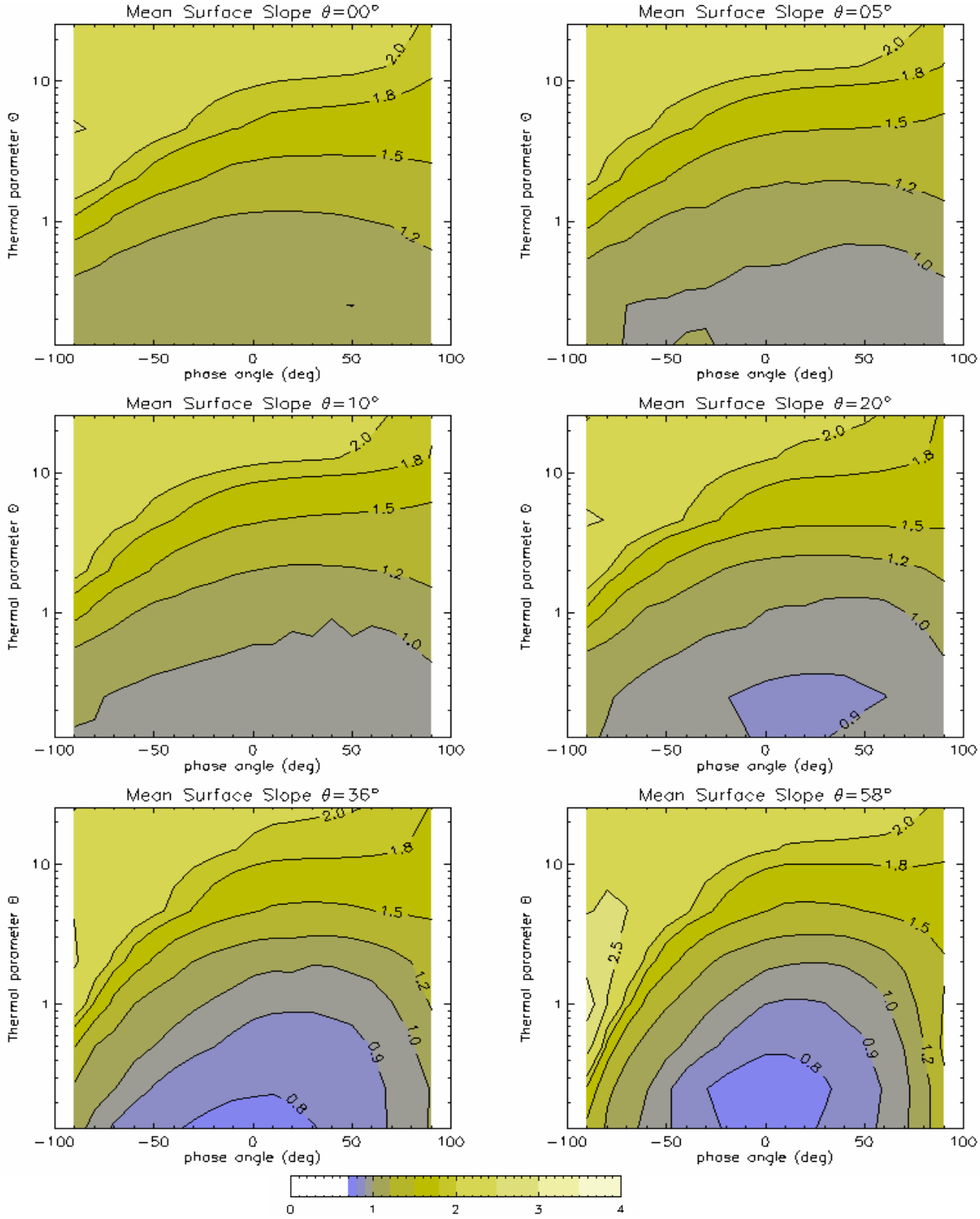

Fig. 6.10 Combined effects of thermal inertia, rotation rate and surface roughness on the theoretical dependence of the NEATM η-value with the phase angle.

6.7 The thermal inertia of NEAs

Not only surface roughness, thermal inertia, and rotation rate contribute to the phase angle dependence of the model parameter η, but the spin vector orientation and the global shape of asteroids are also important. Results that we have discussed here are based on thermophysical model calculations carried out with the asteroid spin vector perpendicular to the plane containing the Sun and the Earth. However, since for most of the observed asteroids in our database with derived η-values, pole direction and shape parameters are not known, we cannot perform detailed thermophysical model calculations for every asteroid to study the thermal inertia and the surface roughness in each case. However, we show that it is possible to derive best-fit thermal properties (mainly the thermal inertia) of averaging the information of all the NEAs in our database on the basis of the scatter plot of their η-values as a function of the phase angle: i.e. the plot of Fig. 5.3.

First of all, we observe that for a given value of Θ and $\overline{\theta}$, when an asteroid is illuminated and observed from a random orientation, the derived η-values are delimited by two curves in the η-α plane. The lower limit is represented by that curve calculated for Θ=0 and macroscopic roughness equal to $\overline{\theta}$, i.e. $\eta(|\alpha|, \Theta=0, \overline{\theta})$, where $|\alpha|$ is the absolute value of α (the curve labeled with "N" of Fig. 6.11). In fact, the hottest temperatures (and thus the lowest η-values) on the surface are reached when its thermal inertia is zero. Furthermore, for Θ=0, the surface temperature distribution is symmetrical with respect to the sub-solar point and consequently the observed color temperature and the derived η-values are a function of $|\alpha|$ only. We show that a negligible error is made by taking the curve than an observer would derive by looking at the morning hemisphere of an asteroid with a rotational axis perpendicular to the plane containing the Sun and the Earth as the upper limit for η. For such geometrical configuration, the phase angle α is always negative: the upper limit curve is thus $\eta(-|\alpha|, \Theta, \overline{\theta})$, the one labeled with "M" in Fig. 6.11. We also call this curve the "morning curve".

To validate this hypothesis, we observe that the surface temperature distributions with the lowest temperatures are obtained when the sub-solar latitude is zero. The smaller the sub-solar latitude is, the wider is the surface of the asteroid over which the incoming solar energy is spread out. However, it is not straightforward that the lowest η-values are observed when the Earth is in the equatorial plane of the asteroid. For instance: is the disk integrated color temperature lower when the morning hemisphere is pointing toward the Earth or when the observer looks straight ahead one of the poles of the object?

To answer this question, we have run our thermophysical model for a number of random orientations of the sub-Earth point and for sub-solar latitude B_{SS}=0, 30, 60 degrees. Results are shown

in Fig. 6.11, where an asteroid with Θ=2.0 and $\bar{\theta}$=36° is simulated. Clearly very few points, only beyond 80° of phase angle, have been found with η-values exceeding that of the morning curve. The assumption that η-values derived for random directions of the asteroid spin vector are constrained by the morning curve (M) and the one of zero thermal inertia have been verified for different degrees of surface roughness and thermal parameter values.

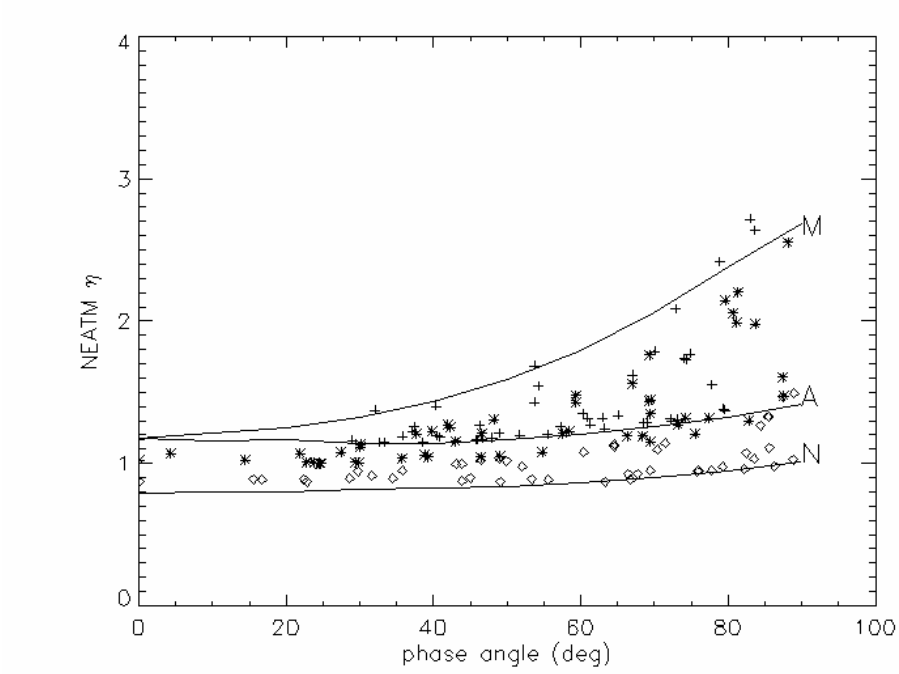

Fig. 6.11 Verification of the hypothesis that η-values derived for asteroids observed from randomly oriented directions are limited by the "morning" curve M and the curve of zero thermal inertia N. The thermophysical model was run for three values of the sub-solar latitude B_{SS}. Crosses represent those η-values derived for asteroids with B_{SS}=0°, asterisks for asteroids with B_{SS}=30° and diamonds for B_{SS}=60°. Note how η-values collapse to the curve of zero thermal inertia as B_{SS} approaches 90°. Following our notation "M" is the curve with $\eta=\eta(-|\alpha|, \Theta, \bar{\theta})$, "A" that with $\eta=\eta(|\alpha|, \Theta, \bar{\theta})$ and "N" that with $\eta=\eta(|\alpha|, \Theta=0, \bar{\theta})$.

So, if we assume that all NEAs had the same value of thermal parameter Θ_{NEA}, and the same degree of surface roughness $\bar{\theta}_{NEA}$, their η-values would be delimited by the morning-curve $\eta(-|\alpha|, \Theta_{NEA}, \bar{\theta}_{NEA})$ and the curve of zero thermal inertia.

However, since the thermal parameter is a function of the asteroid rotation rate, T_{SID}, there is no physical reason to believe that NEAs with very different value of T_{SID} might have the same value of Θ. But, if we are interested to derive a best-fit value (a mean value, so to say) of the thermal inertia Γ_{AVE}, we can calculate the variations of the thermal parameter Θ with respect to the rotational period and the asteroid surface temperature.

$$d\Theta = \frac{\partial \Theta}{\partial T_{SID}} dT_{SID} + \frac{\partial \Theta}{\partial T} dT = -\frac{\sqrt{2\pi}\Gamma_{AVE}}{\varepsilon\sigma T^3} T_{SID}^{-\frac{3}{2}} dT_{SID} - 3\frac{\Gamma\sqrt{2\pi}}{\sqrt{T_{SID}}\varepsilon\sigma T^4} dT \qquad (6\text{-}13)$$

where we have assumed that dT is equal to the difference between the observed color temperature and that implied by the EM (from Eq 5-1):

$$dT = T_{eq}\left(1 - \eta^{-1/4}\right). \qquad (6\text{-}14)$$

dT_{SID} was set as equal to the difference between the actual rotational period of the asteroid and a reference period of six hours. As $d\Theta$ was calculated for each asteroid, final corrections to the measured η-values, $d\eta$, were estimated by interpolation of the numerically evaluated function $\eta(\alpha, \Theta, \bar{\theta})$. This function was previously evaluated (see Eq 6-10 and section 6.6.3) on a fixed grid of points in the α-Θ-$\bar{\theta}$ space. For those asteroids with unknown rotational period, $d\eta$ was assumed equal to 0. Correction factors to the measured η-values were found in most of the cases smaller than the formal errors affecting η-value determinations. Since this correction procedure is another source of errors, we decided to apply correction factors to measured η-values if they were found larger than the η error bars. η-corrected data points are shown with red symbols in Fig. 6.12 and Fig. 6.13 plots.

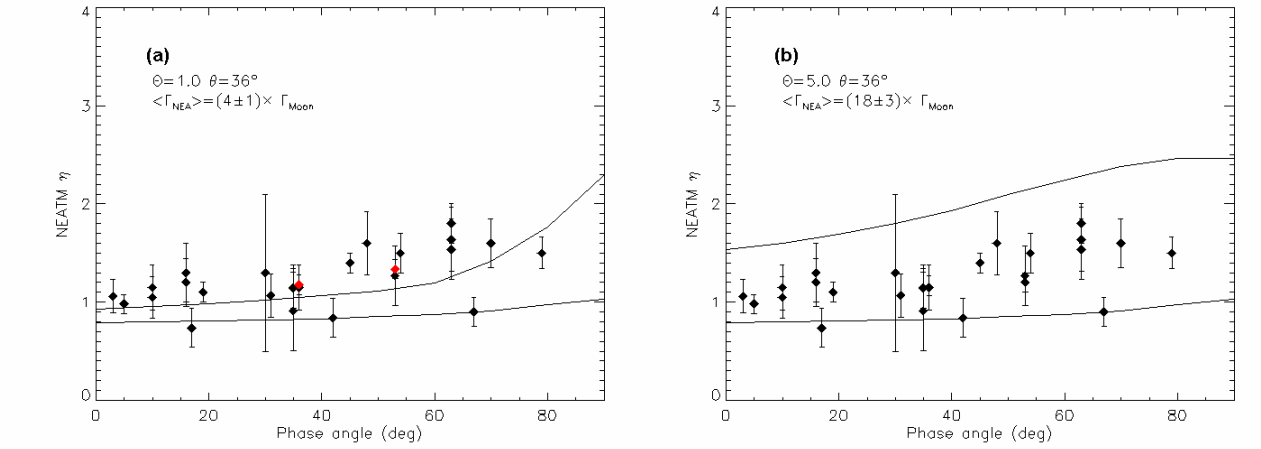

Fig. 6.12 Limiting curves in the Θ-α plane which do not fit properly the observed η-values. See Fig. 6.13 caption for a description of the symbols.

We have finally looked for that set of curves giving the best fit to the observed η-values. Fig. 6.12-a shows how a Θ value too small generates curves which do not fit properly the data. Fig. 6.12-b, on the other hand, demonstrates the opposite effect of using a Θ value too large: data points are not well constrained by the upper limit morning curve.

An appropriate value for the thermal parameter which produces curves delimiting the observed distribution of η values is Θ~3.0. Values ranging from 2.8 up to 3.5 are also compatible with the observations. Unfortunately, constraining the degree of the surface roughness is more difficult and values for $\bar{\theta}$ ranging from 10° up to 36° are in agreement with the observed η-values (see Fig. 6.13).

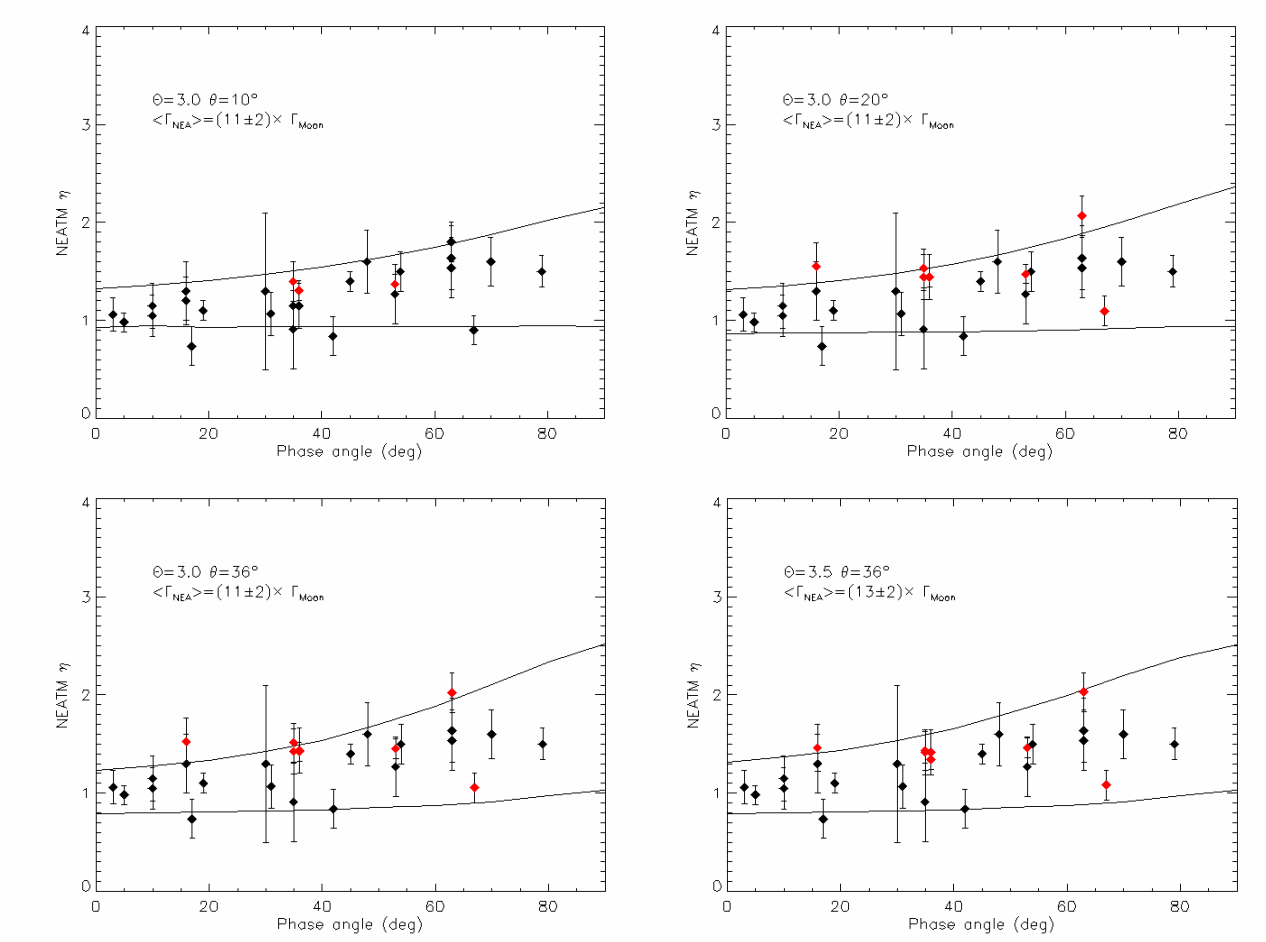

Fig. 6.13 Limiting curves in the η-α plane which DO fit the observed η-values. η-values derived from observations are shown as black diamonds. Data points which η-values have been corrected to the mean rotational period of 6 hours are shown in red colors. The values of the Θ and the $\bar{\theta}$ parameter used to draw the curves are shown on the upper left side of each plot. For each value

Assuming that all NEAs with observed η-values enclosed by the curves of Fig. 6.13 have the same thermal parameter, taking into account the different rotational rates, we derive a best-fit thermal inertia $\Gamma=(550\pm100)$ J m^{-2} s$^{-0.5}$ K^{-1}, or about eleven times that of the Moon which is roughly estimated between 40 and 50 J m^{-2} s$^{-0.5}$ K^{-1} (Harris and Lagerros, 2002 and references therein).

Only those NEAs with "common" thermal properties (see section 5.3.2) have been included in this analysis, separating out those asteroids with anomalously high η-values (see section 5.3.1) and the NEA 5381 Sekmeth. For this latter case, there are six η-values derived from observations made during a single apparition. It is clear that in such a case the hypothesis of random orientation of the spin vector with respect the Sun and the observer is no longer valid and the resulting value of the best-fit thermal inertia of NEAs would have been biased by including Sekmeth's results. However, Fig. 6.14 shows that if the spin axis of the NEA 5381 was perpendicular to the plane containing the Sun and the Earth at the time of the observations, it is very likely that the morning hemisphere of the asteroid was pointing towards the observer and its thermal inertia of the order of some 13 times that of the Moon. It is clear that with more accurate thermophysical model calculations, taking into account the spin vector orientation and the global shape of this object, which at the time of writing are not known, the above results may be refined much further.

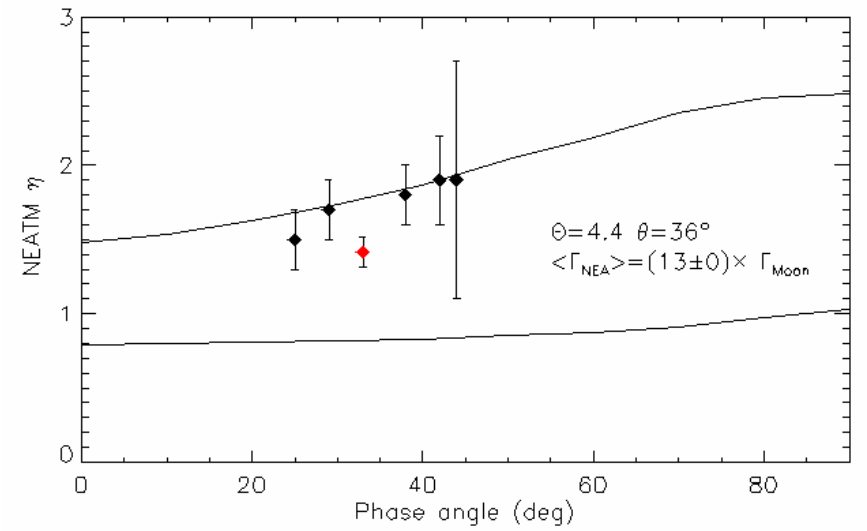

Fig. 6.14 Limiting η-α curves to fit observed η-values of 5381 Sekmeth. Those curves were calculated for Θ=4.4 and $\overline{\theta}$ =36°. See Fig. 6.13 caption for a description of the symbols.

There are few estimations of the thermal inertia for asteroids and in particular for NEAs. The fact that the STM has proven to be successful in the determination of diameters and albedos of large main belt asteroids is an indication of their low thermal inertia. Müller et al. (1999) derived a thermal inertia of 15 J $m^{-2}s^{-0.5}$ K^{-1} for the asteroid 1 Ceres. Müller and Lagerros (2002) proved this value to give thermophysical model results in agreement with observations of other main belt asteroids. Müller and Blommaert (2003) used successfully this value to analyze multi instrument multi epoch thermal infrared observations of the asteroid 65 Cybele. In general, values between 5 and 25 J $m^{-2}s^{-0.5}$ K^{-1} are expected to

apply for a few of the largest main-belt asteroids (Müller and Lagerros, 1998). These values are in good agreement with previous determinations of the thermal inertia of main belt asteroids: Spencer et al. (1989) derived thermal inertia smaller than 30% that of the Moon for 1 Ceres and 2 Pallas and suggested that this value can be applied to other large main belt asteroids.

However, Veeder et al. (1989) have analyzed radiometric observations of 22 NEAs and found for five of these objects the STM to give albedos well above the range expected for their spectral classes. Veeder et al. assumed that this discrepancy is due to some small asteroids having relatively high-thermal-inertia surfaces, resulting from the lack of an insulating layer of regolith, and the failure of the STM to describe their thermal characteristics adequately. Harris and Davies (1999) by combining NEATM results from thermal infrared observations obtained at the UKIRT and previously published data by Lebofsky and Rieke (1979) of the NEA 433 Eros derived a thermal inertia of 170 J $m^{-2}s^{-0.5}$ K^{-1}, or about three times that of the Moon. Given all possible sources of uncertainties, this value is not too far from previous estimations of Morrision (1976), who derived a thermal inertia not larger than 105 J $m^{-2}s^{-0.5}$ K^{-1} for this asteroid. It is worth to note that our method applied to 433 Eros only gives a value of Γ not smaller than 4 times the thermal inertia of the Moon (see Fig. 6.15). The discrepancy with Morrison's result may be due to the fact that he did not take into account roughness effects leading to a lower limit on its value of the asteroid thermal inertia.

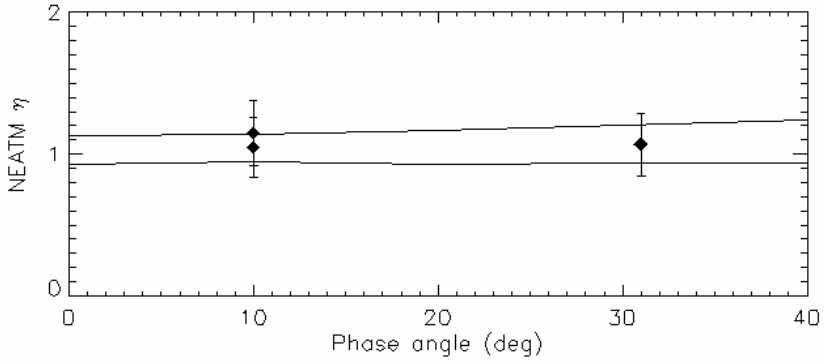

Fig. 6.15 Limiting η-α curves to fit observed η-values of 433 Eros. Those curves were calculated for Θ=1.0 and $\overline{\theta}$ =20°

The case of asteroids with η-values larger than 2 still remains puzzling. The η value of 2100 Ra-Shalom of about 2 at α=40° corresponds to a thermal parameter between 4 and 7, assuming a macroscopic surface $\overline{\theta}$ =36° and that the cooler morning hemisphere of the asteroid was facing the observer in both observing circumstances. Given the very slow rotational period of about 20h, Fig. 6.5 leads us to estimate a very high thermal inertia value between 1500 and 2500 J m^{-2} $s^{-0.5}$ K^{-1}. Assuming

that the afternoon side was pointed towards the observer, an even higher thermal inertia is required to account for the observed low color temperature of the object.

It is very difficult to explain the very high η found for 3671, 2002 BM_{26} and 1999 NC_{43} in terms of the model here developed. Our model can not predict η values that high for $\alpha \approx 60^{o}$. The effect of the global shape of the objects on the thermal inferred emission and on the observed color temperature at high phase angles might explain the observed large η-values. Delbò and Harris (2002) discussed the case of 6489 Golevka for which the radiometric diameter of 350 m derived by Mottola et al. (1997) is in disagreement with the radar diameter obtained by Hudson et al. (2000), who had derived a size of 0.35 $\times$ 0.25 $\times$ 0.25 kilometers. The explanation for the inconsistency probably lies in the effect of shadowing and the extreme geometry at the time of the observation. Give the availability of the three-dimensional radar shape for this asteroid, the thermophysical model described in this chapter may be used to further investigate this problem. However, if the degree of surface roughness and/or the value of the thermal inertia required are unrealistic, then perhaps more sophisticated thermal models including the effect of positive and negative relief and the effect of lateral heat conduction may be necessary.

6.8 Implications for the Yarkovsky effect on kilometer and sub-kilometer size asteroids

The best-fit value we have derived for the thermal inertia of NEAs has important implications to constrain the strength of the Yarkovsky effect of kilometer and sub-kilometer sized asteroids. The Yarkovsky effect is a thermal radiation force that causes objects to undergo semimajor axis drift and spinup/spindown as a function of their spin, orbit, and material properties (see Bottke et al. 2002 and references therein). Surface thermal characteristics, in particular the thermal conductivity and thus thermal inertia, affect the strength of the Yarkovsky effect. Farinella et al. (1998) have shown that the semimajor axis drift rates are function of the thermal parameter Θ. In particular, they have considered three possible values of the surface thermal inertia for meteoritic material and small asteroidal objects in the range $0.2m \leq D \leq 200m$. They have used Γ=12500 J $m^{-2}s^{-0.5}$ K^{-1} for iron rich fragments, Γ=2500 J $m^{-2}s^{-0.5}$ K^{-1} for bare basalt fragments and Γ=39 J $m^{-2}s^{-0.5}$ K^{-1} for regolith-covered fragments. This latter value roughly corresponds to the value of thermal inertia derived for the lunar soil. They have derived maximum semimajor axis drift rates of 2×10^{-5}, 2×10^{-4} and 1.5×10^{-3} AU/Myr respectively, for objects with a diameter of 200 m and a rotational period of 5 hours at 2 AU from the Sun. For such objects, Fig. 2.3 shows that the sub-solar temperature is about 300K. We derive that their thermal parameters Θ are respectively 152, 30.5 and 0.5.

However, if such objects have thermal characteristics similar to that of NEAs, their thermal inertia should have a value Γ_{NEA} of about 500 J m^{-2} $s^{-0.5}$ K^{-1}. Consequently, the thermal parameter for a rotational period of 5 hours and a surface temperature of 300K is $\Theta \approx 6.0$.

Following Farinella et al., the drift in semimajor axis for a near circular orbit is:

$$\dot{a} = 2 f_Y / n \tag{6-15}$$

where f_Y is the along track component of the Yarkovsky force per unit mass and n is the orbital mean motion. By combining Eq (5) and Eq (6) of Farinella et al, it is possible to write f_Y in terms of the thermal parameter Θ:

$$f_Y = \frac{2}{\rho_b R} \frac{\varepsilon \sigma T^4}{c} 0.667 \frac{\Theta}{(1 + 2.03\Theta + 2.04\Theta^2)} f(\zeta) \tag{6-16}$$

where ϱ_b is the material bulk density, c the speed of light, ε the infrared emissivity, σ the Stefan-Boltzman constant, T the temperature and ζ the obliquity of the spin axis. For the diurnal Yarkovsky effect we have $f(\zeta)=\cos(\zeta)$. We can easily calculate the maximum drift rate of an object with NEA-like thermal inertia by taking the ratio of its f_Y with one of the f_Y-values evaluated by Farinella et al. for a different value of the thermal parameter. For instance if we take the ratio of $f_Y(\Theta=6)/f_Y(\Theta=30.5)$ we have that:

$$\dot{a}_{\Theta=6} = \left[\frac{\Theta}{(1 + 2.03\Theta + 2.04\Theta^2)} \right]_{\Theta=6} \Bigg/ \left[\frac{\Theta}{(1 + 2.03\Theta + 2.04\Theta^2)} \right]_{\Theta=30.5} \times \dot{a}_{\Theta=30.5} \tag{6-17}$$

Substituting numerical values into Eq (6-15), we obtain a semimajor axis drift of about 9×10^{-4} AU/Myr for an object with NEA-like thermal inertia with a diameter of 200 m, a rotational period of 5 hours at 2 AU from the Sun.

6.9 Effects of surface roughness, thermal inertia and rotation rate on the accuracy of NEA radiometric diameters and albedos.

Spencer et al. (1989) and Spencer (1990) have shown that thermal inertia and rotation rate has important effects on the thermal emission of asteroids. Systematic errors in radiometric diameters and albedos are likely to occur if simple thermal models, which do not take into account properly those effects, are used.

On the basis of thermophysical model calculations, they have estimated biases in radiometric diameters and albedos derived by the "refined" STM (with the assumption of constant η=0.756) as a

function of the thermal parameter Θ, heliocentric distance and sub-solar latitude (see Fig. 8 and Fig. 9 in Spencer et al. 1989). These errors can be as large as 40 - 50% in diameter if Θ is very large (Θ>1) and the object very dark. Moreover, by assuming a constant value of η, diameters and albedos derived by mean of the STM are likely to include systematic biases especially as a function of the heliocentric distance. Spencer et al. (1998) Fig. 8 shows that for Θ~3, i.e. the mean value we have derived for the large majority of NEAs, radiometric diameters derived by the STM are likely to be between 40 and 20% smaller than the true value. However, Spencer et al. studies were devoted to estimate systematic errors in asteroid diameters derived by the use of the STM only. Moreover, they did not consider what the likely effects of thermal inertia, rotation rate and surface roughness are on the thermal emission of asteroids observed in near Earth space at phase angles as large as 80°.

We have used our thermophysical model to study systematic errors in diameters and albedos derived by the STM as a function of the phase angle for different values of the thermal parameter Θ and degrees of the macroscopic surface roughness. To this end, we have fitted the STM to the N-band data only (i.e. at 8.0, 10.3 and 12.5 μm) of the synthetically generated spectra calculated every 10° of phase angle, from -90° to 90° varying Θ and $\overline{\theta}$ parameters as described in section 6.5 and section 6.6. Fig. 6.16 shows the percentage of the albedo relative error: i.e. the difference between the radiometrically derived and the true albedo dived by the latter.

Our simulation show that accuracy of the STM used with fixed a η value equal to 0.756 is strongly depended on the phase angle and on the thermal parameter and this dependence varies, eventually, with the roughness of the surface. For low degrees of roughness ($\overline{\theta}$ <20°) STM albedo is always larger than the true value. This systematic error, which can be clearly identified by comparing STM with radar diameters (see section 5.5) can be as large as 50 – 100% in the albedo for typical values of the thermal parameter in the case of NEAs (1≤Θ≤5). For larger values of $\overline{\theta}$, the error function becomes very variable within the studied range of phase angles and thermal parameters. In such cases, STM albedos can become smaller the true ones, provided observations of objects with low thermal parameter are carried out at low phase angle. Fig. 6.16 suggests that if we restrict the use of the STM within ±45° of phase angle and if the thermal parameter is not larger than ~2, radiometric albedos are accurate to within ±30%.

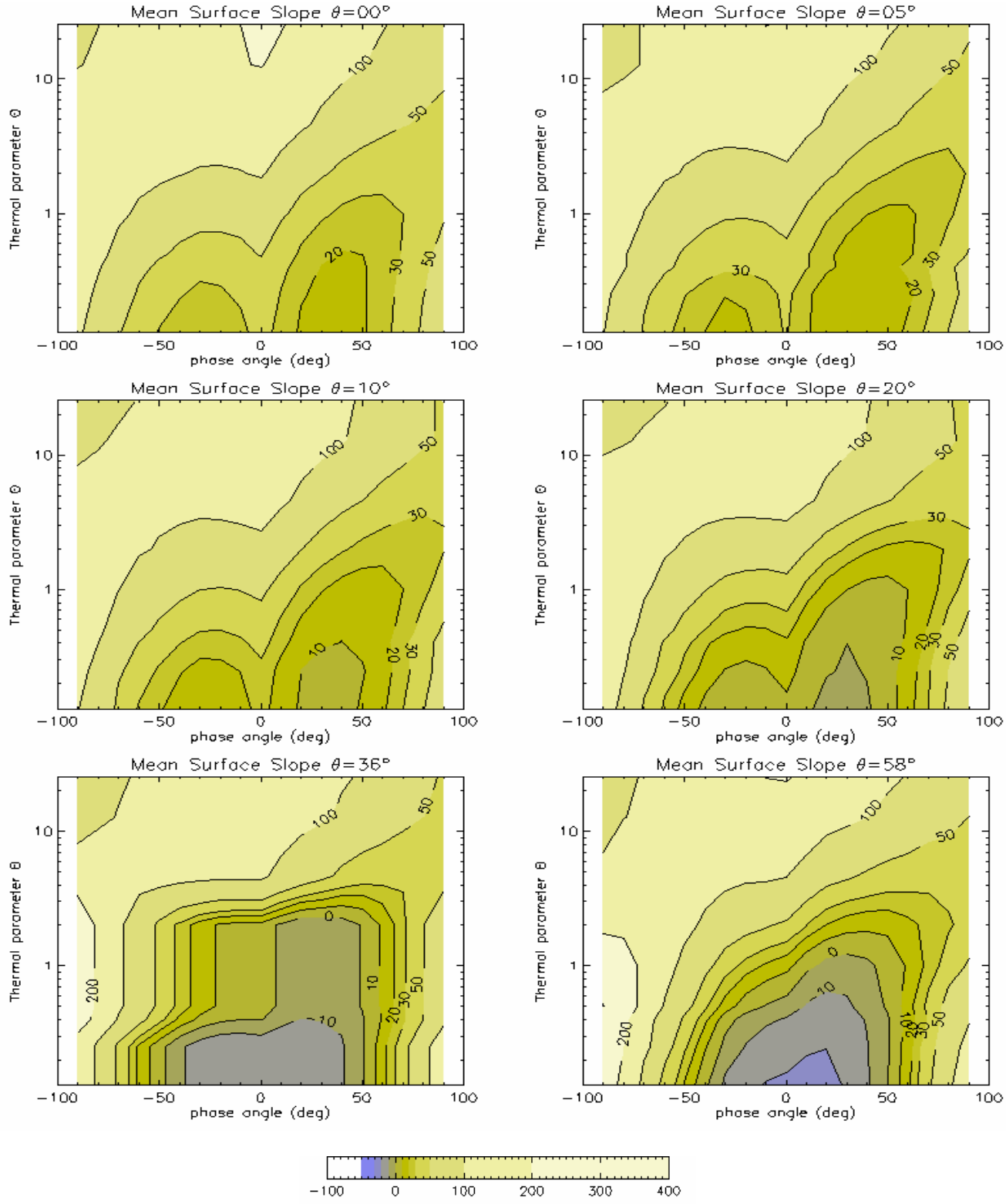

Fig. 6.16 Section of the STM relative albedo error function i.e. $(p_{V\_STM}(\alpha,\Theta, \bar{\theta})-p_{V\_TM})/p_{V\_TM}\times 100$ at constant value of $\bar{\theta}$. The refined STM of Lebosfky and Spencer (1989) was used with constant η=0.756 and β_E=0.01 magnitudes per degree. The function was numerically evaluated on a grid of ten degree of step size in α and at Θ=[0.13, 0.25, 0.40, 0.50, 1.00, 2.00, 4.60, 12.70, 25.5].

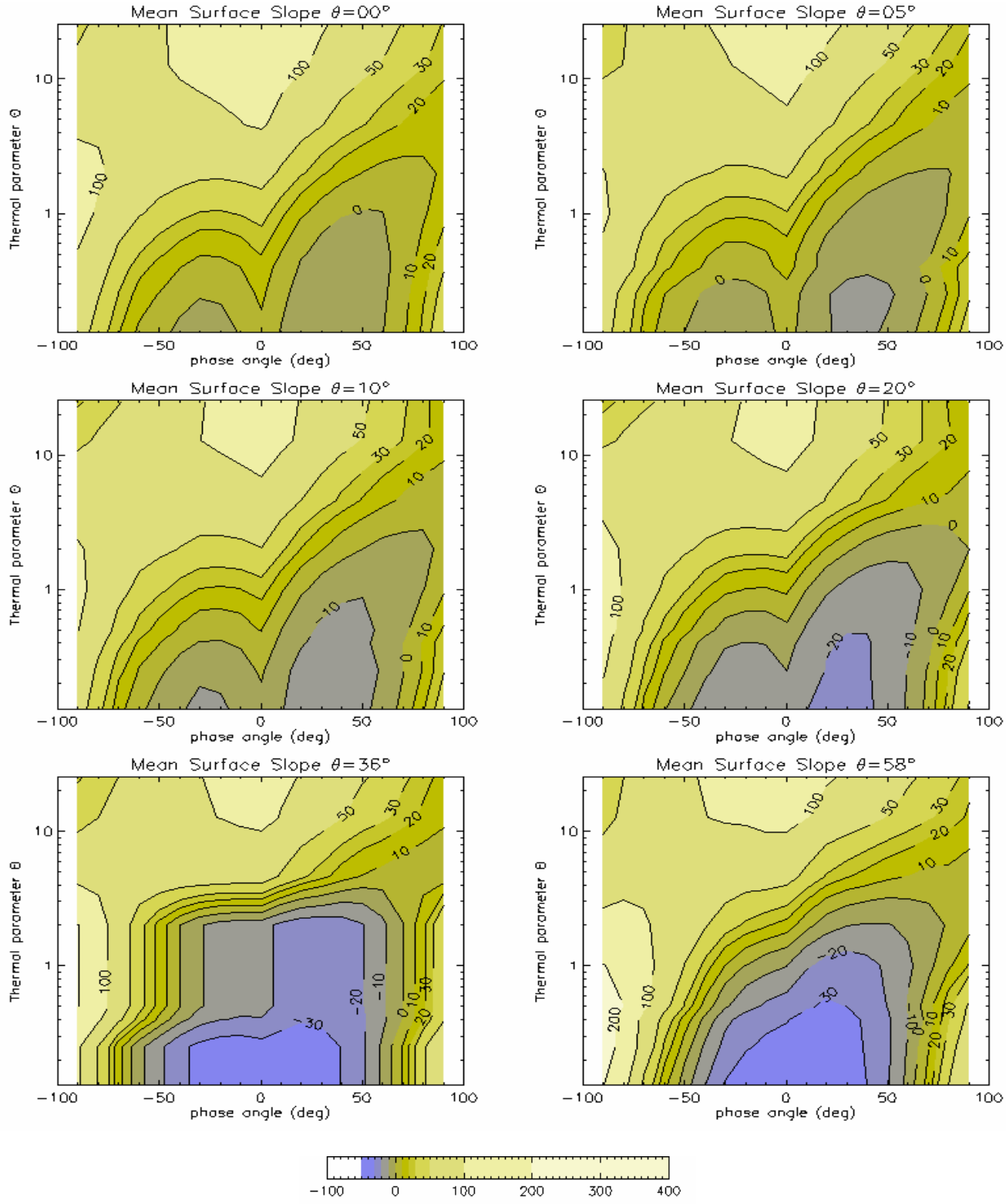

Fig. 6.17 Section of the STM relative albedo error function i.e. $(p_{V\_STM}(\alpha,\Theta,\ \bar{\theta})-p_{V\_TM})/p_{V\_TM}\times 100$ at constant value of $\bar{\theta}$. In contrast to Fig. 6.16, here η is constant but equal to 0.95 and β_E=0.015 magnitudes per degree, as described in section 5.6. The function was numerically evaluated on a grid of ten degree of step size in α and at Θ=[0.13, 0.25, 0.40, 0.50, 1.00, 2.00, 4.60, 12.70, 25.5].

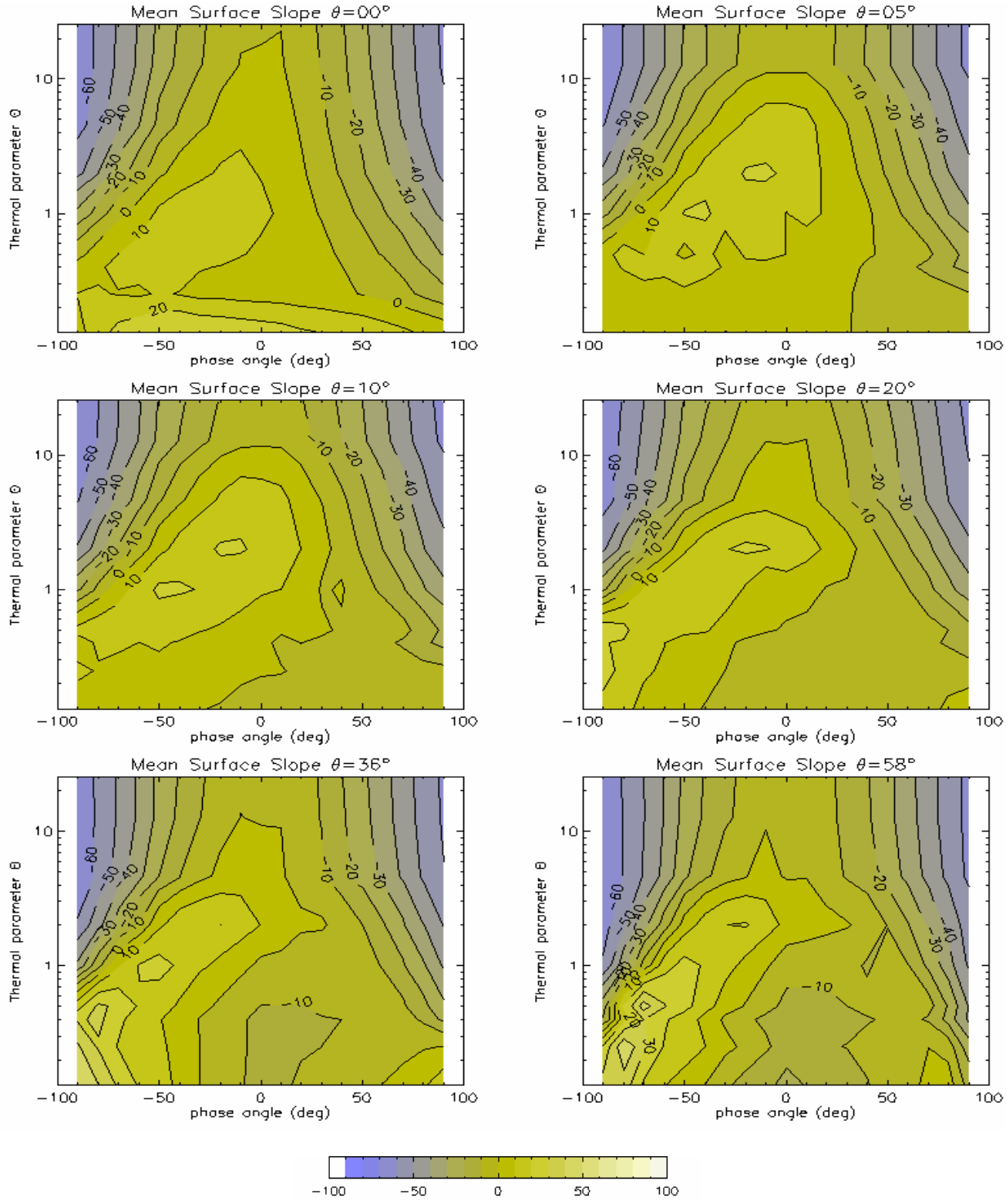

Fig. 6.18 Section of the NEATM relative albedo error function i.e. $(p_{V\_NEATM}(\alpha,\Theta,\bar{\theta})-p_{V\_TM})/\ p_{V\_TM}\times 100$ at six different constant values of $\bar{\theta}$. The function was numerically evaluated on a grid of ten degree of step size in α and at Θ=[0.13, 0.25, 0.40, 0.50, 1.00, 2.00, 4.60, 12.70, 25.5]

Fig. 6.17 shows that a slight improvement of the STM when used with NEAs can be obtained by increasing the η-value to about 0.95 and the infrared phase coefficient β_E to 0.015 magnitudes/degree as we have derived in section 5.6 by comparing STM diameter to radar ones.

Finally, we may note that Fig. 6.16 suggests that STM errors are at minimum in the case of the thermal infrared observations of 433 Eros discussed by Harris & Lagerros (2002), and reported in table 2 of their paper. The STM effective diameter of 20.5 and 21.0 km are in very good agreement the with the size derived by the NEAR Shoemaker spacecraft (D_{eff}(max)=20.6 km). Those observations where obtained at phase angles of 10 and 31 degrees, respectively. Our thermophysical model calculations indicate a thermal parameter Θ of about one and a macroscopic surface roughness $\overline{\theta}$ of about 20°. This latter value is in very good agreement with the estimates obtained from measurements carried out with the near-infrared spectrometer on board the NEAR Shoemaker spacecraft which yielded $\overline{\theta}$ =24±2°. For that range of phase angle and for Θ~1 and $\overline{\theta}$ =20°, Fig. 6.16 indicate an albedo error of +10%.

In section 6.5 and section 6.6, we have used the NEATM to fit synthetic thermal infrared spectra generated by means of our thermophysical model. NEATM solves simultaneously for the η-value, the diameter and the geometric visible albedo. Not only the η-value is thus a function of the phase angle α, of the thermal parameter Θ and of the macroscopic surface roughness $\overline{\theta}$, but also the derived diameter and albedo, in general, depends on those parameter. Along with the best fit parameter η, the diameter and the albedo were derived for each point of the α-Θ-$\overline{\theta}$ space as described in chapter 6.5 and chapter 6.6.

Fig. 6.18 is the analogue of Fig. 6.16 and Fig. 6.17 for the NEATM and shows the albedo relative error, i.e. the difference between the radiometrically derived and the true albedo dived by the latter, in percent. Some irregularities in the curve are artifacts of the finite resolution of the model - we have used a mesh made of only 184 tiles in order to speed up calculations - and are also due to the fairly coarse grid spacing in the α-Θ space.

The non symmetrical shapes of the curves in Fig. 6.18 with respect α=0° is due to the so-called morning-afternoon effect. According to our notation, for negative values of phase angle, the observer looks at the cooler morning side of the asteroid, whereas at phase angle larger than zero the warmer afternoon hemisphere is directed toward the observer. This shows that not only the NEATM derived color temperature, but also the accuracy of radiometric diameter and albedos depends on whether the morning or the afternoon hemisphere of the asteroid is observed. We remind here that diameter and

albedos are related by Eq (2-16) via the absolute magnitude H of the object: given the error on the albedo, it is straightforward to estimate the error on the diameter.

The model error is a rather complicated function of the phase angle, the thermal parameter and the degree of roughness of the surface. However, some general behavior of this function can be found even if thermal inertia, rotation rate and surface roughness are not known. In Fig. 6.19, we have plotted the relative albedo error as a function of the η-value for observations carried out at low or moderate phase angle ($-40° \leq \alpha \leq 40°$, Fig. 6.19, a) and at large phase angle ($|\alpha| \geq 40°$,Fig. 6.19, b).

In the first case we can easily see that the error on albedo is very rarely larger than $\pm 20\%$. Moreover, for η-values smaller than 1.1 a correlation η vs. model error appears such that NEATM underestimate the albedo of objects with higher color temperatures (i.e. smaller η-values). For η-values larger than 1.1 the correlation goes the other way and objects which appear hotter are likely to have albedos overestimated by the NEATM.

In the case of observations at large phase angle the scatter in Fig. 6.19, b) is much larger and for $\eta <\sim 1.2$ it appears that no correlation of the model error with the color temperature can be found. However, for larger η-values ($\eta > 1.5$) NEATM is likely to underestimate the albedo and consequently to overestimate the diameter. This error is mainly due to the fact that the NEATM ignores the thermal emission arising from the night side. This error increases with increasing η and increasing solar phase angle.

The general shape of the model error function plotted in Fig. 6.18 indicates that NEATM gives reliable results in the case on NEAs if their thermal parameters are neither not too high, nor too low ($0.1 \leq \Theta \leq 5$) and the phase angle not too extreme ($|\alpha| < 60°$).

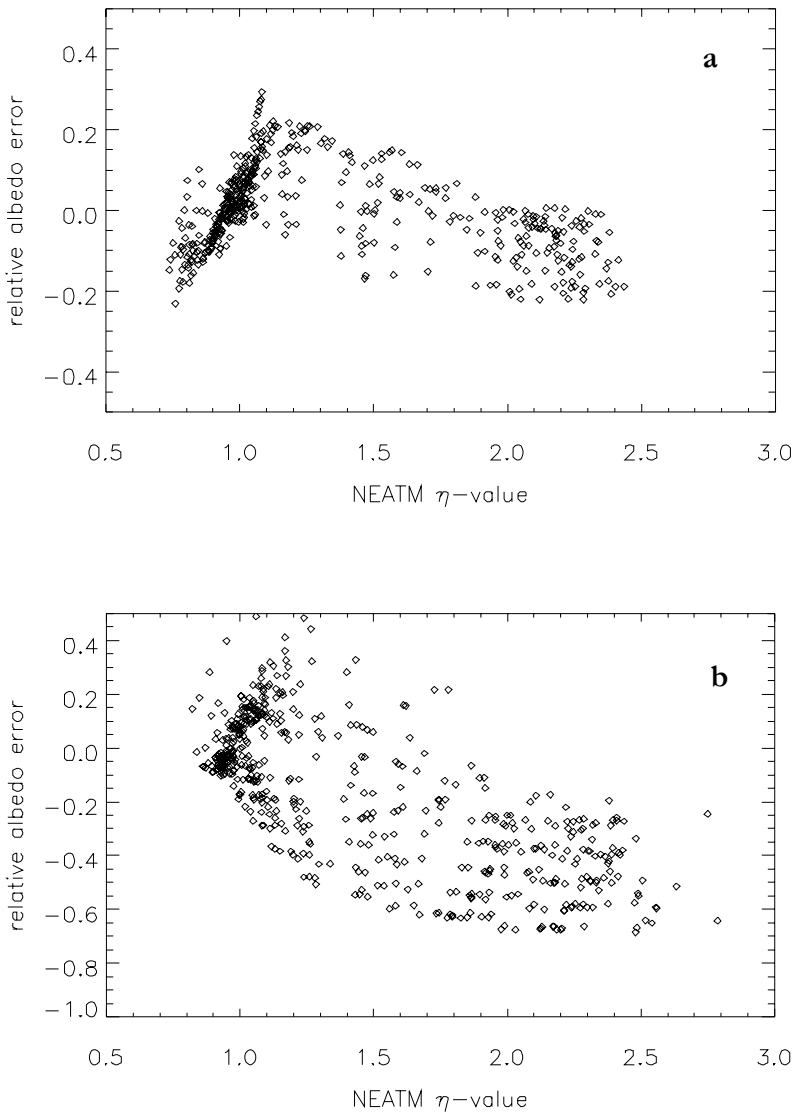

Fig. 6.19 Distribution of the albedo relative error as a function of the η-value for asteroid observed at phase angle between -40 and 40 degrees (a) and at phase angle larger than 40° or smaller than -40°.

6.10 Conclusions

In this chapter we have described a thermophysical model which can generate thermal infrared spectra taking into account the combined effect of rotation rate, pole orientation, thermal inertia and surface roughness. We have used this model with synthetic spherical asteroids; however, the implementation here described allows the use of general convex shapes.

Thermal inertia has been modeled by numerically solving the equation of vertical heat transport, whereas surface roughness has been modeled by means of spherical section craters which density and opening angle can be adjusted. The effect of surface characteristics on the thermal radiation of asteroids can be described in terms of the thermal parameter Θ and the mean surface slope $\overline{\theta}$ which gives the degree of macroscopic roughness on the surface.

We have used the thermophysical model to study the dependence of the NEATM best fit η parameter for different illumination and observing geometries as a function of the thermal parameter Θ and the mean surface slope $\overline{\theta}$. In particular we devoted great interest to model the effect of the phase angle. Indeed, information on the thermal inertia and some hints on the degree of surface roughness of NEAs may be obtained from the study of the variation of the η-value, with solar phase angle.

Although the NEATM derived η-value is a complicated function of all those parameters, we have demonstrated that for a given value of Θ and $\overline{\theta}$, for random orientations of the asteroid spin vectors with respect to the Sun and the observer, η-values are constrained by two curves: the curve of zero thermal inertia and the "morning curve" obtained by looking at the morning hemisphere of an asteroid with a rotational axis perpendicular to the plane containing the Sun and the Earth.

We have searched for that set of curves giving the best fit to the observed distribution of η-values. We found that a thermal inertia Γ=550±100J m^{-2} $s^{-0.5}$ K^{-1} gives the best fit to the large majority of the observations in our data set. This value is about eleven times the thermal inertia derived for the lunar soil. Surface roughness is not very well constrained and values of the mean surface slope between 20 and 35° are in good agreement with the observations.

Our thermophysical model cannot explain the very low color temperature observed for NEAs 3671, 2002 BM_{26} and 1999 NC_{43}. Perhaps more sophisticated thermal models including the effect of positive and negative relief and the effect of lateral heat conduction may be necessary in those cases.

However, our thermophysical model derives values in good agreement with the findings of other researchers for the thermal inertia the mean surface slope of 433 Eros.

The relatively high η-values derived for the NEA 5381 Sekmeth are explained with a thermal parameter Θ~4 which implies a thermal inertia thirteen times that of the moon and a high degree of surface roughness ($\overline{\theta}$ ~36°). The variation of the η-value 5381 Sekmeth with phase angle is compatible our thermophysical model calculations if the cool mooring side of the object has been observed.

The derived average value of the NEA thermal inertia put constrains on the strength of the Yarkovsky effect on kilometer and sub-kilometer size bodies. We obtain a semimajor axis drift rate of about 9×10^{-4} AU/Myr for an object with NEA-like thermal inertia with a diameter of 200 m, a rotational period of 5 hours at 2 AU from the Sun.

With our thermophysical model we have studied the effects of surface roughness, thermal inertia and rotation rate on the accuracy of NEA radiometric diameters and albedos.

Our simulations show that the accuracy of the STM used with fixed a η value equal to 0.756 is strongly depended on the phase angle. However, if we restrict its use to within $\pm45°$ of phase angle and if the thermal parameter is not larger than ~2, radiometric albedos are accurate to within $\pm30\%$. We argue that the refinement to the STM proposed in section 5.6 reduces model errors for its use with NEAs.

In the case of the NEATM the error on albedo is very rarely larger than $\pm20\%$ for observations obtained to within $\pm40°$ of phase angle. A correlation of the model error with η-value can bee seen for both the case of observations obtained at small phase angles and for those carried out at large phase angle. In this latter case η-values larger than 1.5 correspond always to an underestimation of the real albedo with this effect increasing for increasing η.